This is an open access article published under an ACS AuthorChoice License, which permits copying and redistribution of the article or any adaptations for non-commercial purposes.

ACS OMEGA

Article

Cite This: ACS Omega 2018, 3, 7832−7839

Water-Stable Nanoscale Zirconium-Based Metal−Organic Frameworks for the Effective Removal of Glyphosate from Aqueous Media

Asha Pankajakshan, Mekhola Sinha, Anupam Anand Ojha, and Sukhendu Mandal*

School of Chemistry, Indian Institute of Science Education and Research Thiruvananthapuram, Maruthamala (P O), Vithura, 695551 Thiruvananthapuram, Kerala, India

Supporting Information

ABSTRACT: Two water-stable zirconium-based metal−organic frameworks (MOFs) (NU-1000 and UiO-67) have been synthesized in various size scales (100−2000 nm) for the adsorptive removal of glyphosate from the aqueous media. Both NU-1000 and UiO-67 possess a three-dimensional structure; NU-1000 consists of triangular micropores and wide mesoporous channels (31 Å), whereas UiO-67 has cage-like pores [octahedral (16 Å) and tetrahedral (14 Å) cages]. NU-1000 comprises $Zr_6(\mu_3\text{-}O)_4(\mu_3\text{-}OH)_4(H_2O)_4(OH)_4$, and UiO-67 contains $Zr_6O_4(OH)_4$ as secondary building units. These units act as Lewis acid nodes and can interact with the Lewis base phosphate group of the glyphosate. The time taken for reaching equilibrium is found to be reduced considerably as the size of the MOF decreases. The smaller the particle size, the lesser is the diffusion barrier for the analyte, which enhances the interaction between Lewis acidic metal nodes and the Lewis basic center of the glyphosate molecule. NU-1000 was found to be better compared to UiO-67, both in terms of efficiency and reusability. This might be due to the larger pore diameters of the NU-1000. Theoretical calculations revealed that the interaction energy of glyphosate with the nodes of NU-1000 is higher (−37.63 KJ mol^{-1}) compared to UiO-67 (−17.37 KJ mol^{-1}), which might be the possible reason for the higher efficiency of NU-1000.

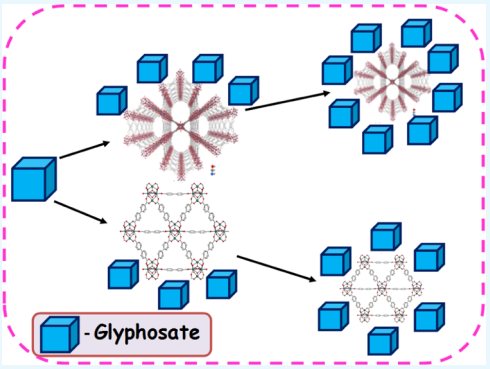

INTRODUCTION

Organophosphorus compounds (OPs) are highly noxious.[1] They not only cause eutrophication but also bind to the neurotransmitter, acetyl cholinesterase, thereby leading to nerve paralysis and death of living beings.[2] OPs enter our drinking water mainly through agricultural runoff.[3] Hence, the removal of OPs from water is very important. There are various ways to eradicate OPs from aqueous media; among those, enzymatic biodegradation, photocatalytic degradation, and adsorption are commonly used.[4,5] Among these methods, adsorption is the simplest and cost-effective way. Metal−organic frameworks (MOFs) are a promising class of porous materials for the adsorptive removal of lethal chemicals.[6,7] The tunable size and shape of the pores, stable framework, and the opportunity for desirable post-synthetic modification can vary the adsorption capacity of the MOFs.[8] Recent findings revealed the possibility of reducing diffusion limitations by downsizing the mesoporous MOFs.[9−11] Therefore, the blend of mesopores in the nano-sized MOF system will engender new-generation materials with enhanced and efficient properties for the applications such as catalysis, adsorption, and so forth.

The MOFs with Zr metal nodes are well-known for the adsorption of analyte molecules containing the phosphate group from aqueous media.[12] The affinity upsurges with the number of the Zr−OH bonds and the missing linker effect.[8a,b] Hence, the MOFs with plenty of Zr−(OH)−Zr bridge bonds resemble the phosphotriesterase enzyme with similar Zn−(OH)−Zn moieties, which degrades the OPs gradually but at a dawdling pace.[13]

Glyphosate is a widely used broad-spectrum herbicide which causes damage to human cells.[14,15] Studies showed that the half-life of glyphosate in soil might extend to months, which increases the risk of erosion and contamination of surface and groundwater sources.[16,17] Once it reaches the water bodies, the half-life increases. Moreover, the possible degradation (hydrolysis) product of glyphosate is aminomethylphosphonic acid which is as equally toxic as glyphosate.[18] Therefore, adsorptive removal of glyphosate from aqueous medium is essential to protect the environment and human health.

Hupp and co-workers have investigated the catalytic activity of NU-1000 and UiO-67 in degrading the chemical warfare agents and/or their simulants. Zr_6 nodes with terminal water and hydroxyl groups were the catalytic sites.[9a,12] It was also shown that the catalytic efficiency escalates as the size of the MOFs reduced to nano-regime, whereby increasing the surface

Received: May 6, 2018
Accepted: June 25, 2018
Published: July 12, 2018

Downloaded via 24.40.129.82 on May 11, 2024 at 13:28:30 (UTC).
See https://pubs.acs.org/sharingguidelines for options on how to legitimately share published articles.

© 2018 American Chemical Society

DOI: 10.1021/acsomega.8b00921
ACS Omega 2018, 3, 7832−7839

area (higher surface to volume ratio).[9] Lange et al. in 2014 reported the adsorptive removal of methyl parathion using a copper MOF from water.[19] In 2015, Zhu et al. have studied the use of UiO-67 in removing the OPs (glyphosate and glufosinate) from the water through the adsorption process.[20]

In this work, synthesis of two zirconium-based MOFs (NU-1000 and UiO-67) in various size ranges (100−2000 nm) have been carried out for the adsorptive removal of the glyphosate from aqueous medium(Scheme 1). We have studied how the

Scheme 1. Synthesis Procedure of the MOFs

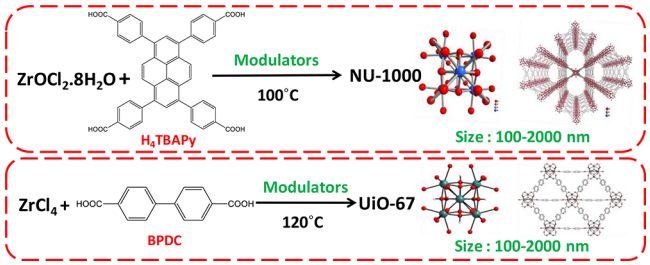

efficiency of adsorption increased as the particle size decreases. It was also shown that the time taken for reaching adsorption equilibrium was considerably diminished as the particle size decreased to the nano-size range and the effect was found more pronounced for NU-1000 over UiO-67. The interaction between the glyphosate and MOFs was probed through XPS and IR data, respectively. Theoretical calculations revealed that the interaction energy of the glyphosate with NU-1000 is 20.26 KJ mol^{-1} higher than that of UiO-67.

RESULTS AND DISCUSSION

We have synthesized NU-1000 and UiO-67 using modified literature methods (see the Supporting Information).[21,22] Structure of the MOFs and glyphosate are given in the Supporting Information (Figure S1). The experimental powder X-ray diffraction data of the synthesized MOFs matched with the simulated data, indicating the phase purity of all the samples (Figure S2). Scanning electron microscopy (SEM) images revealed the formation of particles with mean sizes ranging from 100 to 2000 nm (Figures 1 and S3). Thermogravimetric analysis showed that the solvent molecules residing in the pores of the structure starts escaping at 75 °C; after that, from 300 °C, the dehydration of $Zr_6O_4(OH)_4$ nodes starts and the structure disintegrates at temperature ≫ 400 °C (Figure S4). The nitrogen adsorption isotherms were showing an upsurge in the surface area, and the pore size distribution plots illustrate the escalation in the pore diameter as the particle size decreases (Figures S5−S7).

NU-1000 comprises eight connected $Zr_6(\mu_3\text{-}O)_4(\mu_3\text{-}OH)_4(H_2O)_4(OH)_4$ nodes interconnected by tetra topic 1,3,6,8 (*p*-benzoate) pyrene ($TBAPy^{4-}$) linkers. UiO-67 is a build-up of 12-connected $Zr_6O_4(OH)_4$ clusters nodes and linear 4,4′-biphenyl dicarboxylic acid (BPDC) ligands. It possesses a face-centered cubic arrangement of the Zr_6 clusters. Both NU-1000 and UiO-67 contain free and bridging −OH and H_2O groups. NU-1000 has wide mesoporous channels (31 Å), and UiO-67 has octahedral (16 Å) and tetrahedral (14 Å) cages (Scheme 1 and Figure S1). The synthesis of NU-1000 and UiO-67 MOFs of different particle sizes was carried out by the coordination modulation method (see the Supporting Information). The synthesized MOFs were used for the systematic study of the removal of toxic glyphosate molecule from water.

The adsorption of glyphosate as a function of particle sizes of NU-1000 and UiO-67 have been carried out under identical conditions (same glyphosate concentration and the amount of MOFs) at room temperature. The supernatants were examined to measure the concentration of elemental phosphorus and zirconium using ICP-AES measurements. Control experiments without the MOFs showed negligible change in the concentration of phosphorus. The absence of zirconium in the supernatant revealed the stability of both the MOFs during the adsorption process. The adsorption percentage as a function of time is shown in Figure 2. It was shown that adsorption efficiency is enhanced with the downsizing of the MOFs, and the effect was more pronounced in case of NU-1000 compared to UiO-67. We have carried out several experiments to probe the interaction between the MOF samples and glyphosate which are discussed below. The MOF samples were analyzed after the adsorption study followed by washing.

The IR spectra of MOFs after the adsorption study have been recorded, and the incorporation of glyphosate was evident from the presence of the characteristics peaks of glyphosate (Figure 3). All the characteristics peaks of the MOFs are red-shifted because of the possible interaction between the MOF and glyphosate. The triplet at 793, 722, and 662 cm^{-1} (labeled with magenta stars) are the peaks corresponding to the Zr−O longitudinal and transverse mode vibrations, respectively. The sharp and intense peaks at 1615 and 1417 cm^{-1} (labeled with red stars) are in- and out-of-plane stretching of the carboxylate groups of the ligand,

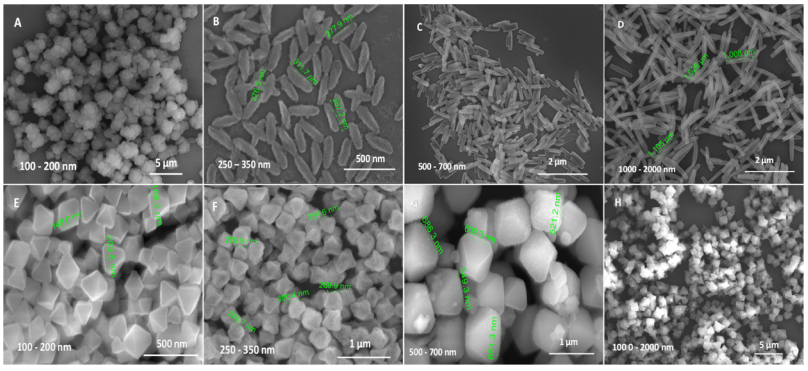

Figure 1. SEM images of NU-1000 (A−D) and UiO-67 (E−H) MOFs of various sizes (ranges from 100 to 2000 nm).

DOI: 10.1021/acsomega.8b00921
ACS Omega 2018, 3, 7832−7839

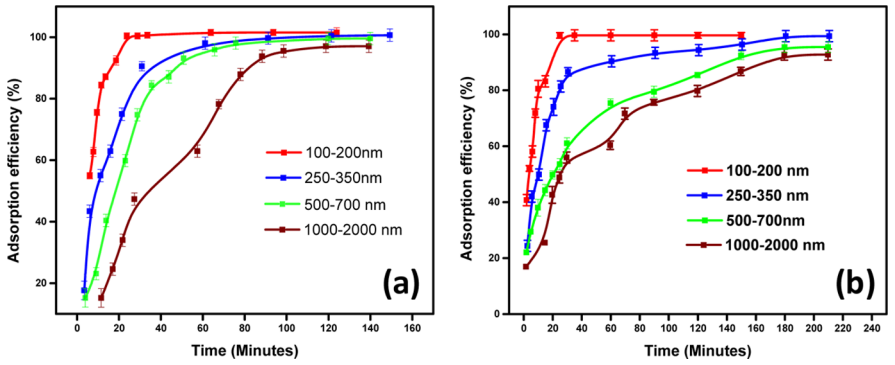

Figure 2. Adsorption efficiency of (a) NU-1000 and (b) UiO-67 MOF samples.

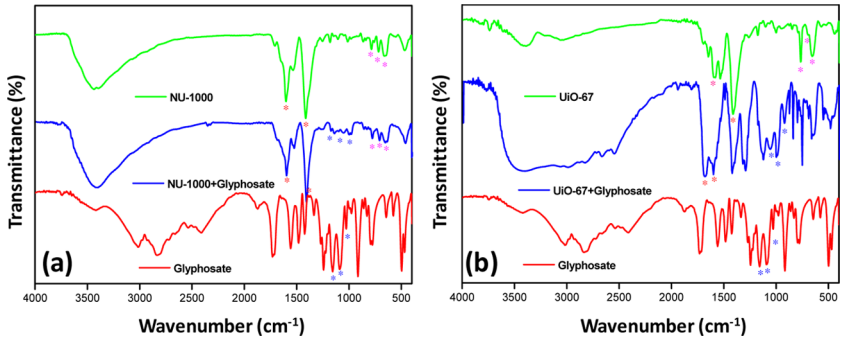

Figure 3. IR spectra of the MOFs (a) NU-1000 and (b) UiO-67 before and after the adsorption studies. Note that only one sample of each NU-1000 and UiO-67 (100−200 nm) is shown.

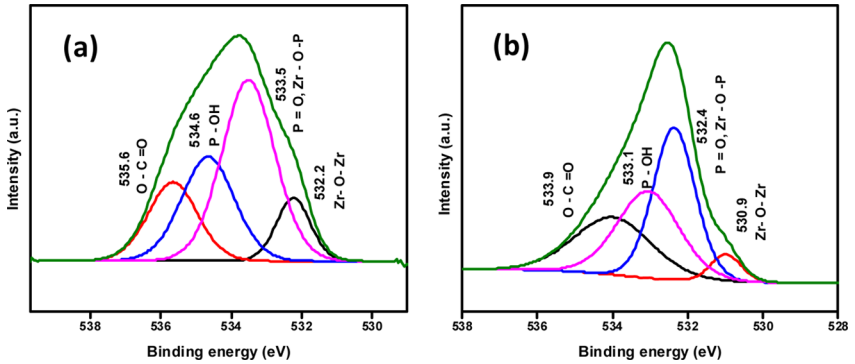

Figure 4. XPS spectrum of the MOFs (a) NU-1000 and (b) UiO-67 after the adsorption studies. Note: only one sample for each NU-1000 and UiO-67 (100−200 nm) is shown.

respectively. The three peaks at 1164, 1100, and 1032 cm^{-1} correspond to the P═O bond and the antisymmetric and symmetric vibrations of P−O in the glyphosate, respectively (labeled with blue stars).[4,20]

All the MOF samples after the adsorption study were analyzed using SEM and SEM−energy-dispersive X-ray spectroscopy (EDXS). It was found that all the samples maintained the structural morphology after the adsorption of glyphosate (Figure S8). The presence of elemental phosphorus confirmed the adsorption indisputably (Figure S9). We have calculated the elemental phosphorus contents in each particle size for both the MOFs, and it was observed that the amount of phosphorus increases as the particles size decreases (Table S1). The SEM−EDX spectrum was re-recorded after washing (washed with water and acetone and then heated at particular temperature under vacuum). The absence of phosphorus peaks confirmed the complete removal of adsorbed glyphosate on washing (Figure S10).

The stability of the washed MOF samples were studied using powder XRD. The NU-1000 MOF retained the structural stability even after washing and is used for three more adsorption cycles. The structural integrity of the UiO-67 samples was lost after washing (Figure S11).

The N_2 adsorption study illustrates that the surface area and the pore diameter of the MOF samples increase with downsizing the MOFs. The enhancement of the rate of removal of glyphosate by nanoscale MOFs might be due to the large external surface area and hence shortened diffusion paths. The surface area of the NU-1000 samples was found to be diminishing after each consecutive cycle. It may be due to the destruction of many of the active sites during the successive activation process after each cycle (Figure S12). In the case of UiO-67, the structure was degraded after the first cycle (Figure

DOI: 10.1021/acsomega.8b00921
ACS Omega 2018, 3, 7832−7839

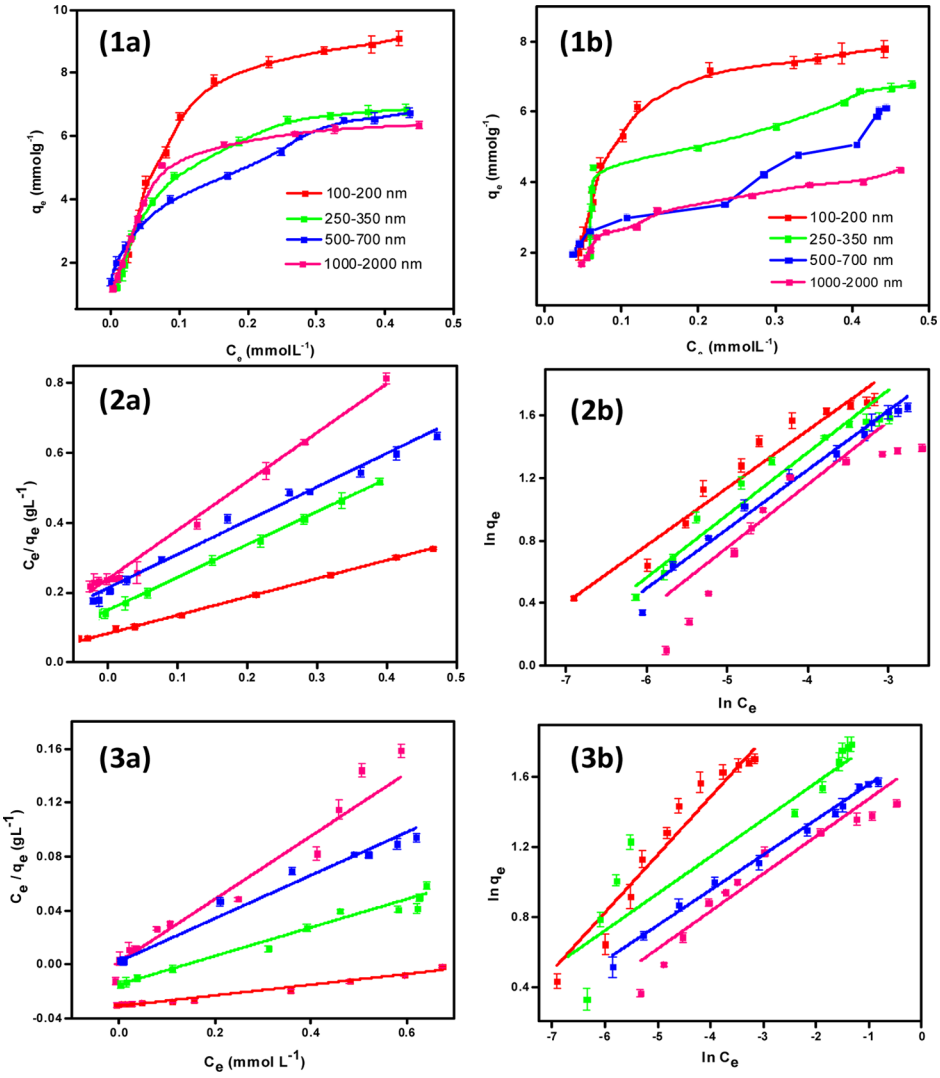

Figure 5. (1) Adsorption isotherms of glyphosate adsorption on the MOFs, the plots of (2) Langmuir model and (3) Freundlich model. Note: (a,b) represents NU-1000 and UiO-67, respectively.

S13). This degradation could be due to the capillary action which leads to the channel collapse during the activation process of UiO-67.

The XPS spectra were collected before and after the adsorption studies (Figures 4 and S14). It shows that the binding energy of Zr−OH_2, Zr−OH, and Zr−O−Zr bonds have shifted after adsorption of glyphosate (Table S2). This evidenced the interaction between the metal nodes of the MOFs and glyphosate.

Mechanism of Adsorption. The adsorption capacity with varying particle sizes as a function of time is provided in Figure 2. The early rapid adsorption in all the cases could be due to the availability of plenty of vacant active sites in the activated MOF structure. Figure 2 shows that the saturation time of adsorption decreases substantially as the size decreases from micro to nanoscale. In the case of NU-1000 with a size range of 100−200 nm, the 50% adsorption took place in about 3 min, while it took almost 9 min for the UiO-67 MOF of similar size to show the same activity. This difference in adsorption capacity between two MOFs was observed with all the particle sizes.

The Zr metal nodes in the framework of both the MOFs act as the adsorption sites for the glyphosate.[23] The Zr metal nodes are Lewis acidic and have a higher affinity for the phosphate functional group of glyphosate which is a Lewis base. It is well-known that the utilization of modulators during the synthesis not only helps to tune the size of the MOF particles but also increases the possibility of formation of missing linker sites. These missing linkers are compensated by the −OH groups which are highly reactive toward organophosphates. As the size of the MOF decreases, the possibility of missing linker formation increases which could be the main reason for the enhancement in the adsorption efficiency.

The adsorption kinetic studies reveals that the pseudo-second order model is more appropriate in explaining the adsorption process where the correlation coefficients and q_e are matching better with the experimental results (Tables S3−S18 and Figures S15−S22). The theory of adsorption with chelating ligands following pseudo-second-order kinetics is widely accepted. Here, the mesoporosity and the carboxylic acid groups in the structure of the MOF make them act as a chelating agent, thereby supporting the pseudo-second-order kinetics.[24−26] The reaction involves three main components, MOF, glyphosate, and the solvent water. Because water is in excess, its concentration can be neglected, thereby supporting pseudo-second-order kinetics.[27−36]

DOI: 10.1021/acsomega.8b00921
ACS Omega 2018, 3, 7832−7839

Table 1. Langmuir and Freundlich Parameters of the MOFs for the Glyphosate Adsorption

	Langmuir model			Freundlich model		
size of the MOF	k_L(L mmol^{-1})	q_{max} (mmol g^{-1})	R^2	k_F (mmol^{n-1} L^n g^{-1})	n	R^2
			NU-1000			
100−200 nm	230.06 ± 0.13	8.97 ± 0.03	0.999	8.91 ± 0.11	0.463 ± 0.17	0.968
250−350 nm	124.90 ± 0.22	6.49 ± 0.05	0.989	4.53 ± 0.06	0.438 ±0.05	0.967
500−700 nm	91.68 ± 0.08	6.37 ± 0.14	0.995	1.94 ±0.04	0.468 ± 0.08	0.725
1000−2000 nm	74.29 ± 0.11	6.05 ± 1.02	0.997	9.52 ± 0.15	0.368 ±0.14	0.987
			UiO-67			
100−200 nm	126.73 ± 12.03	7.90 ± 1.02	0.997	13.53 ±0.12	0.546 ± 0.023	0.951
250−350 nm	71.49 ±7.56	6.12 ± 0.08	0.999	8.12 ± 0.07	0.204 ± 0.006	0.710
500−700 nm	50.92 ±5.38	5.44 ±0.02	0.989	6.45 ±0.03	0.331 ±0.012	0.990
1000−2000 nm	70.25 ± 5.68	3.21 ± 0.02	0.995	2.95 ± 0.06	0.482 ± 0.014	0.892

The adsorption isotherms for the glyphosate adsorption (both the Langmuir and Freundlich models) on the MOFs are provided in Figure 5. The obtained parameters and the correlation coefficients are presented in Table 1. It was found that the Langmuir model has a better fit than the Freundlich model in all the cases. This proved that MOF surfaces are homogeneous in nature, where the adsorption sites are uniformly distributed. The maximum adsorption capacity is found to be more for NU-1000 samples compared to UiO-67. Moreover, it is clear that as the size of the MOF decreases, the adsorption capacity increases. We have compared the adsorption coefficient with the reported results, and it shows that the adsorption coefficient of these nanoscale MOFs is higher compared to the reported materials in the literature (Table 2).

The higher efficiency of the NU-1000 compared to that of UiO-67 can be explained by considering the structural uniqueness of NU-1000, as adsorption competence is mainly determined by the likelihood of contact between the adsorbent and the adsorbate and the diffusion pathway. The wide hexagonal pores of diameter 31 Å in NU-1000 allow the glyphosate solution to have better interactions with the metal nodes. The improved efficiency is supported by the theoretical calculations as well. Theoretical calculations showed that the adsorption energy for glyphosate on NU-1000 is −37.63 KJ mol^{-1}, while that for UiO-67 is only −17.37 kJ mol^{-1}. The negative values of adsorption energies indicate a strong interaction of the glyphosate with the Zr clusters of the MOFs. Also, the Zr···O−P interatomic distance during the polar interaction in the case of NU-1000 was found to be 4.2 Å, while it is 4.6 Å for UiO-67. The higher adsorption energy and the shorter Zr···O−P distance indicates a stronger interaction of glyphosate with NU-1000 over UiO-67 (Figure S23).[37−41]

Table 2. Comparison of the Adsorption Capacities of Glyphosate by Various Adsorbents

adsorbents		q_{max} (mmol g^{-1})	reference
NU-1000	100−200 nm	8.97	this work
	250−300 nm	6.49	
	500−700 nm	6.37	
	1000−2000 nm	6.05	
UiO-67	100−200 nm	7.90	this work
	250−300 nm	6.12	
	500−700 nm	5.44	
	1000−2000 nm	3.21	
Fe_3O_4@SiO_2@UiO-67		1.52	26
$MnFe_2O_4$−graphene		0.23	27
MnO_x/Al_2O_3		0.69	28
dendro biochar		0.26	29
UiO-67		3.18	20
chitosan/alginate membrane		4.73×10^{-5}	30
polyaniline/ZSM-5		0.58	31
montmorillonite		0.295	32
alum sludge		0.67	33
Ni_2AlNO_3		1.02	34
α-FeOOH		0.23	35
MgAl-LDH		1.09	36

CONCLUSIONS

The synthesis of two Zr-based MOFs (NU-1000 and UiO-67) in various size ranges from nanometer to micrometer have been carried out. The presence of the Zr_6 cluster with the terminal H_2O molecule and the −OH group makes these clusters active sites for specific adsorption. We have exploited the affinity of the Lewis acidic Zr metal centers in the corresponding MOFs toward the phosphate group in the pesticide glyphosate for its adsorptive removal from aqueous media. Theoretical calculations revealed that glyphosate has higher interactions with NU-1000 compared to UiO-67, and it is because of the high adsorption energy and the lower Zr···O−P distance. Kinetic studies show that the adsorption follows pseudo-second-order kinetics. The saturation time of the adsorption decreases dramatically as the particle size decreases from micron to nano-regime. This enhancement in the adsorption rate and capacity might be due to the increase in the external surface area and reduction in the diffusion barrier. This outcome of size-dependent properties of MOFs may inspire people/other research groups to synthesize new nanoscale mesoporous MOFs for various other applications.

EXPERIMENTAL SECTION

Adsorption Studies. A stock solution of the glyphosate with a concentration of 9.879 mmol L^{-1} was prepared in water. The adsorption capacity of the MOFs was tested using the glyphosate solution (50 mL, 0.01 mmol L^{-1}) with 3 mg of activated MOFs for 5 h. The supernatant was collected at certain intervals of time and the change in the concentration of glyphosate was investigated by measuring the amount of phosphorus using ICP-AES. Control experiments without MOFs were also carried out. The concentration of the elemental zirconium was measured to check the disintegration

DOI: 10.1021/acsomega.8b00921
ACS Omega 2018, 3, 7832−7839

of the MOFs during the study. The adsorption study was repeated three times to obtain reproducible results.

The adsorption kinetic experiments were carried out using glyphosate solution (50 mL, 0.1 mmol L^{-1}) with 10 mg of MOF samples. The solution was kept in a mechanical shaker and rotated at a speed of 180 rpm for 300 min. The supernatant was collected at regular intervals, and the amounts of adsorbed glyphosate were measured from the difference between the initial (C_0) and equilibrium (C_e) concentrations in the supernatant after centrifugation. The equilibrium uptake was calculated by the given equation

$$q_e = (C_0 - C_e)\frac{V}{W} \quad (1)$$

where q_e (mmol g^{-1}) is the equilibrium adsorption capacity of the glyphosate on the MOF samples. V is the volume of the glyphosate solution used (L), and W is the weight of the MOF sample (g). Experimental kinetic data were fitted with the pseudo-first-order and pseudo-second-order models. The pseudo-first-order equation is given by

$$\log_{10}(q_e - q_t) = \log_{10} q_e - \frac{k_1 t}{2.303} \quad (2)$$

where q_e and q_t are the amounts of glyphosate adsorbed by the MOF at equilibrium and at the time, t, respectively. k_1 is the pseudo-first-order rate constant (min^{-1}). Plotting $\log_{10}(q_e - q_t)$ as a function of time, t gives a straight line, and the value of k_1 can be calculated from its slope.

For the pseudo-second-order model, the equation used is

$$\frac{t}{q_t} = \frac{1}{k_2 q_e^2} + \frac{t}{q_e} \quad \text{(type 1)} \quad (3)$$

$$q_e = \frac{1}{\text{slope}}; k_2 = \frac{(\text{slope})^2}{\text{intercept}}$$

where q_e and q_t are the same as above and k_2 is the pseudo-second-order rate constant (g $mmol^{-1}$ min^{-1}). When t/q_t is plotted against time, t a linear plot is obtained. The values of q_e and k_2 can be calculated from the slope and the intercept of the straight line.

Adsorption Isotherms. The adsorption isotherms for the adsorption of glyphosate on the MOFs was obtained at 25 °C. The maximum shaking time was 300 min. Two widely used isotherm models, Langmuir and Freundlich models, were employed to simulate the adsorption. The linear equation for the Langmuir adsorption model is

$$\frac{C_e}{q_e} = \frac{1}{k_L q_{max}} + \frac{C_e}{q_{max}} \quad (4)$$

where k_L represents the Langmuir constant (L $mmol^{-1}$) that relates to the energy of adsorption and affinity of the binding sites and q_{max} represents the maximum adsorption capacity of the adsorbent (mmol g^{-1}).

The linear form of the Freundlich adsorption isotherm equation is

$$\log q_e = \log k_F + n \log C_e \quad (5)$$

where k_F is the Freundlich adsorption constant ($mmol^{1-n}$ L^n g^{-1}) that relates to the adsorption capacity of the adsorbent and n is the adsorption intensity.

Theoretical Studies. Theoretical calculations have been carried out to find the interaction energy between the Zr MOF and the glyphosate molecule. The stability of the Zr cluster−glyphosate system was calculated from the adsorption energy using the given equation

$$E_{adsorption} = E_{total} - (E_{cluster} + E_{glyphosate}) \quad (6)$$

where E_{total} is the energy of the system consisting of the Zr cluster and glyphosate and $E_{cluster}$ and $E_{glyphosate}$ represent the energies of the isolated Zr cluster and glyphosate, respectively.

■ ASSOCIATED CONTENT

Supporting Information

The Supporting Information is available free of charge on the ACS Publications website at DOI: 10.1021/acsomega.8b00921.

Materials and methods, structures, all characterization data, adsorption data, absorption data, and kinetic data with modeling (PDF)

■ AUTHOR INFORMATION

Corresponding Author

*E-mail: sukhendu@iisertvm.ac.in (S.M.).

ORCID

Sukhendu Mandal: 0000-0002-4725-8418

Funding

Science and Engineering Research Board (SERB), Govt. of India, through a grant EMR/2016/007501.

Notes

The authors declare no competing financial interest.

■ ACKNOWLEDGMENTS

We acknowledge SAIF IITB for ICP-AES data. P.A. acknowledges CSIR for SRF.

■ REFERENCES

(1) Eddleston, M.; Buckley, N. A.; Eyer, P.; Dawson, A. H. Management of acute organophosphorus pesticide poisoning. *Lancet* **2008**, *371*, 597−607.

(2) (a) Vera, M. S.; Lagomarsino, L.; Sylvester, M.; Pérez, G. L.; Rodríguez, P.; Mugni, H.; Sinistro, R.; Ferraro, M.; Bonetto, C.; Zagarese, H.; Pizarro, H. New evidences of roundup (glyphosate formulation) impact on the periphyton community and the water quality of freshwater ecosystems. *Ecotoxicology* **2010**, *19*, 710−721. (b) Marrs, T. C. Organophosphate poisoning. *Pharmacol. Ther.* **1993**, *58*, 51−66.

(3) Moss, B. Water pollution by agriculture. *Philos. Trans. R. Soc., B* **2008**, *363*, 659−666.

(4) Daou, T. J.; Begin-Colin, S.; Grenèche, J. M.; Thomas, F.; Derory, A.; Bernhardt, P.; Legaré, P.; Pourroy, G. Phosphate adsorption properties of magnetite-based particles. *Chem. Mater.* **2007**, *19*, 4494−4505.

(5) Cycoń, M.; Żmijowska, A.; Wójcik, M.; Piotrowska-Seget, Z. Biodegradation of the organophosphorus insecticide diazinon by serratia sp. and pseudomonas sp. and their use in bioremediation of contaminated soil. *J. Environ. Manage.* **2013**, *117*, 7−16.

(6) (a) Zhang, Q.; Yu, J.; Cai, J.; Zhang, L.; Cui, Y.; Yang, Y.; Chen, B.; Qian, G. A porous Zr-cluster-based cationic metal-organic framework for highly efficient $Cr_2O_7^{2-}$ removal from water. *Chem. Commun.* **2015**, *51*, 14732−14734. (b) Dias, E. M.; Petit, C. Towards the use of metal-organic frameworks for water reuse: A review of the recent advances in the field of organic pollutants removal and degradation and the next steps in the field. *J. Mater. Chem. A* **2015**, *3*,

DOI: 10.1021/acsomega.8b00921
ACS Omega 2018, 3, 7832−7839

22484−22506. (c) Wang, B.; Lv, X.-L.; Feng, D.; Xie, L.-H.; Zhang, J.; Li, M.; Xie, Y.; Li, J.-R.; Zhou, H.-C. Highly Stable Zr(IV)-Based Metal-Organic Frameworks for the Detection and Removal of Antibiotics and Organic Explosives in Water. *J. Am. Chem. Soc.* **2016**, *138*, 6204−6216.

(7) (a) Seo, P. W.; Bhadra, B. N.; Ahmed, I.; Khan, N. A.; Jhung, S. H. Adsorptive removal of pharmaceuticals and personal care products from water with functionalized metal-organic frameworks: remarkable adsorbents with hydrogen bonding abilities. *Sci. Rep.* **2016**, *6*, 34462−34472. (b) Wang, C.; Liu, X.; Chen, J. P.; Li, K. Superior removal of arsenic from water with zirconium metal-organic framework UiO-66. *Sci. Rep.* **2015**, *5*, 16613−16622. (c) Luo, X.; Ding, L.; Luo, J. Adsorptive Removal of Pb(II) Ions from Aqueous Samples with Amino-Functionalization of Metal-Organic Frameworks MIL-101(Cr). *J. Chem. Eng. Data* **2015**, *60*, 1732−1743.

(8) (a) de Voorde, B. V.; Stassen, I.; Bueken, B.; Vermoortele, F.; de Vos, D.; Ameloot, R.; Tan, J.-C.; Bennett, T. D. Improving the mechanical stability of zirconium-based metal-organic frameworks by incorporation of acidic modulators. *J. Mater. Chem. A* **2015**, *3*, 1737−1742. (b) Kalidindi, S. B.; Nayak, S.; Briggs, M. E.; Jansat, S.; Katsoulidis, A. P.; Miller, G. J.; Warren, J. E.; Antypov, D.; Corà, F.; Slater, B.; Prestly, M. R.; Martí-Gastaldo, C.; Rosseinsky, M. J. Chemical and Structural Stability of Zirconium-based Metal-Organic Frameworks with Large Three-Dimensional Pores by Linker Engineering. *Angew. Chem., Int. Ed.* **2015**, *54*, 221−226. (c) Furukawa, H.; Gándara, F.; Zhang, Y.-B.; Jiang, J.; Queen, W. L.; Hudson, M. R.; Yaghi, O. M. Water Adsorption in Porous Metal-Organic Frameworks and Related Materials. *J. Am. Chem. Soc.* **2014**, *136*, 4369−4381. (d) Burtch, N. C.; Jasuja, H.; Walton, K. S. Water Stability and Adsorption in Metal-Organic Frameworks. *Chem. Rev.* **2014**, *114*, 10575−10612.

(9) (a) Liu, Y.; Moon, S.-Y.; Hupp, J. T.; Farha, O. K. Dual-function metal-organic framework as a versatile catalyst for detoxifying chemical warfare agent simulants. *ACS Nano* **2015**, *9*, 12358−12364. (b) López-Maya, E.; Montoro, C.; Rodríguez-Albelo, L. M.; Aznar Cervantes, S. D. A.; Lozano-Pérez, A. A.; Cenís, J. L.; Barea, E.; Navarro, J. A. R. Textile/Metal-Organic-Framework Composites as Self-Detoxifying Filters for Chemical-Warfare Agents. *Angew. Chem., Int. Ed.* **2015**, *54*, 6790−6794. (c) Katz, M. J.; Moon, S.-Y.; Mondloch, J. E.; Beyzavi, M. H.; Stephenson, C. J.; Hupp, J. T.; Farha, O. K. Exploiting parameter space in MOFs: a 20-fold enhancement of phosphate-ester hydrolysis with UiO-66-NH_2. *Chem. Sci.* **2015**, *6*, 2286−2291.

(10) (a) Liu, G.; Lin, Y. Electrochemical sensor for organophosphate pesticides and nerve agents using zirconia nanoparticles as selective sorbents. *Anal. Chem.* **2005**, *77*, 5894−5901. (b) Katz, M. J.; Mondloch, J. E.; Totten, R. K.; Park, J. K.; Nguyen, S. T.; Farha, O. K.; Hupp, J. T. Simple and compelling biomimetic metal-organic framework catalyst for the degradation of nerve agent simulants. *Angew. Chem., Int. Ed.* **2014**, *53*, 497−501.

(11) (a) Chen, Y.; Xiong, Z.; Peng, L.; Gan, Y.; Zhao, Y.; Shen, J.; Qian, J.; Zhang, L.; Zhang, W. Facile preparation of core-shell magnetic metal-organic framework nanoparticles for the selective capture of phosphopeptides. *ACS Appl. Mater. Interfaces* **2015**, *7*, 16338−16347. (b) Ziem, B.; Azab, W.; Gholami, M. F.; Rabe, J. P.; Osterrieder, N.; Haag, R. Size-dependent inhibition of herpesvirus cellular entry by polyvalent nanoarchitectures. *Nanoscale* **2017**, *9*, 3774−3783.

(12) Moon, S.-Y.; Wagner, G. W.; Mondloch, J. E.; Peterson, G. W.; DeCoste, J. B.; Hupp, J. T.; Farha, O. K. Effective, facile, and selective hydrolysis of the chemical warfare agent VX using Zr_6-based metal−organic frameworks. *Inorg. Chem.* **2014**, *54*, 10829−10833.

(13) (a) Ghanem, E.; Raushel, F. Detoxification of organophosphate nerve agents by bacterial phosphotriesterase. *Toxicol. Appl. Pharmacol.* **2005**, *207*, 459−470. (b) Benning, M. M.; Kuo, J. M.; Raushel, F. M.; Holden, H. M. Three-Dimensional structure of Phosphotriesterase: An enzyme capable of detoxifying organophosphate nerve agents. *Biochemistry* **1994**, *33*, 15001−15007. (c) Aubert, S. D.; Li, Y.; Raushel, F. M. Mechanism for the Hydrolysis of Organophosphates by the Bacterial Phosphotriesterase†. *Biochemistry* **2004**, *43*, 5707−5715.

(14) (a) Hertwich, E. G.; Mateles, S. F.; Pease, W. S.; McKone, T. E. Human toxicity potentials for life-cycle assessment and toxics release inventory risk screening. *Environ. Toxicol. Chem.* **2001**, *20*, 928−939. (b) Benachour, N.; Séralini, G.-E. Glyphosate formulations induce apoptosis and necrosis in human umbilical, embryonic, and placental cells. *Chem. Res. Toxicol.* **2009**, *22*, 97−105. (c) Richard, S.; Moslemi, S.; Sipahutar, H.; Benachour, N.; Seralini, G.-E. Differential Effects of Glyphosate and Roundup on Human Placental Cells and Aromatase. *Environ. Health Perspect.* **2005**, *113*, 716−720.

(15) (a) Williams, G. M.; Kroes, R.; Munro, I. C. Safety Evaluation and Risk Assessment of the Herbicide Roundup and Its Active Ingredient, Glyphosate, for Humans. *Regul. Toxicol. Pharmacol.* **2000**, *31*, 117−165. (b) De Roos, A. J.; Blair, A.; Rusiecki, J. A.; Hoppin, J. A.; Svec, M.; Dosemeci, M.; Sandler, D. P.; Alavanja, M. C. Cancer incidence among glyphosate-exposed pesticide applicators in the agricultural health study. *Environ. Health Perspect.* **2005**, *113*, 49−54.

(16) Todorovic, G. R.; Mentler, A.; Rampazzo, N.; Blum, W. E.; Eder, H. A.; Strauss, P. Dispersion of glyphosate in soils undergoing erosion. *Environ. Qual.* **2010**, *4*, 15−28.

(17) Lima, I. S.; Baumeier, N. C.; Rosa, R. T.; Campelo, P. M. S.; Rosa, E. A. R. Influence of glyphosate in planktonic and biofilm growth of pseudomonas aeruginosa. *Braz. J. Microbiol.* **2014**, *45*, 971−975.

(18) (a) Zaranyika, M. F.; Nyandoro, M. G. Degradation of glyphosate in the aquatic environment: An enzymic kinetic model that takes into account microbial degradation of both free and colloidal (or sediment) particle adsorbed glyphosate. *J. Agric. Food Chem.* **1993**, *41*, 838−842. (b) https://en.wikipedia.org/wiki/Aminomethylphosphonic_acid.

(19) Lange, L. E.; Ochanda, F. O.; Obendorf, S. K.; Hinestroza, J. P. CuBTC metal-organic frameworks enmeshed in polyacrylonitrile fibrous membrane remove methyl parathion from solutions. *Fibers Polym.* **2014**, *15*, 200−207.

(20) Zhu, X.; Li, B.; Yang, J.; Li, Y.; Zhao, W.; Shi, J.; Gu, J. Effective adsorption and enhanced removal of organophosphorus pesticides from aqueous solution by Zr-Based MOFs of UiO-67. *ACS Appl. Mater. Interfaces* **2015**, *7*, 223−231.

(21) (a) Wang, T. C.; Vermeulen, N. A.; Kim, I. S.; Martinson, A. B.; Stoddart, J. F.; Hupp, J. T.; Farha, O. K. Scalable synthesis and post-modification of a mesoporous metal-organic framework called NU-1000. *Nat. Protoc.* **2016**, *11*, 149−162. (b) Li, P.; Klet, R. C.; Moon, S.-Y.; Wang, T. C.; Deria, P.; Peters, A. W.; Klahr, B. M.; Park, H.-J.; Al-Juaid, S. S.; Hupp, J. T.; Farha, O. K. Synthesis of nanocrystals of Zr-based metal-organic frameworks with csq-net: significant enhancement in the degradation of a nerve agent simulant. *Chem. Commun.* **2015**, *51*, 10925−10928.

(22) (a) Fei, H.; Cohen, S. M. A robust, catalytic metal-organic framework with open 2,2′-bipyridine sites. *Chem. Commun.* **2014**, *50*, 4810−4812. (b) Katz, M. J.; Brown, Z. J.; Colón, Y. J.; Siu, P. W.; Scheidt, K. A.; Snurr, R. Q.; Hupp, J. T.; Farha, O. K. A facile synthesis of UiO-66, UiO-67 and their derivatives. *Chem. Commun.* **2013**, *49*, 9449−9451. (c) Gutov, O. V.; Hevia, M. G.; Escudero-Adán, E. C.; Shafir, A. Metal-Organic Framework (MOF) Defects under Control: Insights into the Missing Linker Sites and Their Implication in the Reactivity of Zirconium-Based Frameworks. *Inorg. Chem.* **2015**, *54*, 8396−8400.

(23) (a) Li, J.; Wang, X.; Zhao, G.; Chen, C.; Chai, Z.; Alsaedi, A.; Hayat, T.; Wang, X. Metal-organic framework-based materials: superior adsorbents for the capture of toxic and radioactive metal ions. *Chem. Soc. Rev.* **2018**, *47*, 2322−2356. (b) Li, J.; Li, X.; Alsaedi, A.; Hayat, T.; Chen, C. Synthesis of highly porous inorganic adsorbents derived from metal-organic frameworks and their application in efficient elimination of mercury(II). *J. Colloid Interface Sci.* **2018**, *517*, 61−71. (c) Zhu, K.; Chen, C.; Xu, H.; Gao, Y.; Tan, X.; Alsaedi, A.; Hayat, T. Cr(VI) Reduction and Immobilization by Core-Double-Shell Structured Magnetic Polydopamine@Zeolitic Idazolate Frameworks-8 Microspheres. *ACS Sustainable Chem. Eng.*

DOI: 10.1021/acsomega.8b00921
ACS Omega 2018, 3, 7832−7839

2017, *5*, 6795−6802. (d) Li, J.; Li, X.; Hayat, T.; Alsaedi, A.; Chen, C. Screening of Zirconium-Based Metal-Organic Frameworks for Efficient Simultaneous Removal of Antimonite (Sb(III)) and Antimonate (Sb(V)) from Aqueous Solution. *ACS Sustainable Chem. Eng.* **2017**, *5*, 11496−11503.
(24) Canepa, P.; Nijem, N.; Chabal, Y. J.; Thonhauser, T. Diffusion of small molecules in metal-organic framework materials. *Phys. Rev. Lett.* **2013**, *110*, 026102−026107.
(25) Ho, Y.; McKay, G. The kinetics of sorption of divalent metal ions onto sphagnum moss peat. *Water Res.* **2000**, *34*, 735−742.
(26) Ho, Y. S.; McKay, G. Pseudo-second order model for sorption processes. *Process Biochem.* **1999**, *34*, 451−465.
(27) Yang, Q.; Wang, J.; Chen, X.; Yang, W.; Pei, H.; Hu, N.; Li, Z.; Suo, Y.; Li, T.; Wang, J. The simultaneous detection and removal of organophosphorus pesticides by a novel Zr-MOF based smart adsorbent. *J. Mater. Chem. A* **2018**, *6*, 2184−2192.
(28) Yamaguchi, N. U.; Bergamasco, R.; Hamoudi, S. Magnetic $MnFe_2O_4$−graphene hybrid composite for efficient removal of glyphosate from water. *Chem. Eng. J.* **2016**, *295*, 391−402.
(29) Zheng, T.; Sun, Y.; Lin, Y.; Wang, N.; Wang, P. Study on preparation of microwave absorbing $MnOx/Al_2O_3$ adsorbent and degradation of adsorbed glyphosate in MW-UV system. *Chem. Eng. J.* **2016**, *298*, 68−74.
(30) Mayakaduwa, S. S.; Kumarathilaka, P.; Herath, I.; Ahmad, M.; Al-Wabel, M.; Ok, Y. S.; Usman, A.; Abduljabbar, A.; Vithanage, M. Equilibrium and kinetic mechanisms of woody biochar on aqueous glyphosate removal. *Chemosphere* **2016**, *144*, 2516−2521.
(31) Carneiro, R. T. A.; Taketa, T. B.; Gomes Neto, R. J. G.; Oliveira, J. L.; Campos, E. V. R.; de Moraes, M. A.; da Silva, C. M. G.; Beppu, M. M.; Fraceto, L. F. Removal of glyphosate herbicide from water using biopolymer membranes. *J. Environ. Manage.* **2015**, *151*, 353−360.
(32) Milojević-Rakić, M.; Janošević, A.; Krstić, J.; Nedić Vasiljević, B.; Dondur, V.; Ćirić-Marjanović, G. Polyaniline and its Composites with Zeolite ZSM-5 for Efficient Removal of Glyphosate from Aqueous Solution. *Micro. Meso. Mater.* **2013**, *180*, 141−155.
(33) Khoury, G. A.; Gehris, T. C.; Tribe, L.; Torres Sánchez, R. M. T.; dos Santos Afonso, M. Glyphosate Adsorption on Montmorillonite: An Experimental and Theoretical Study of Surface Complexes. *Appl. Clay Sci.* **2010**, *50*, 167−175.
(34) Hu, Y. S.; Zhao, Y. Q.; Sorohan, B. Removal of glyphosate from aqueous environment by adsorption using water industrial residual. *Desalination* **2011**, *271*, 150−156.
(35) Khenifi, A.; Derriche, Z.; Mousty, C.; Prévot, V.; Forano, C. Adsorption of Glyphosate and Glufosinate by Ni_2AlNO_3 layered double hydroxide. *Appl. Clay Sci.* **2010**, *47*, 362−371.
(36) Jonsson, C. M.; Persson, P.; Sjöberg, S.; Loring, J. S. Adsorption of Glyphosate on Goethite (α-FeOOH): Surface Complexation Modeling Combining Spectroscopic and Adsorption Data. *Environ. Sci. Technol.* **2008**, *42*, 2464−2469.
(37) Li, F.; Wang, Y.; Yang, Q.; Evans, D. G.; Forano, C.; Duan, X. Study on Adsorption of Glyphosate (N-Phosphonomethyl Glycine) Pesticide on MgAl-Layered Double Hydroxides in Aqueous Solution. *J. Hazard. Mater.* **2005**, *125*, 89−95.
(38) Yael, J. A.; Fuhr, J. D.; Bocan, G. A.; Millone, A. D.; Tognalli, N.; Afonso, M. d. S.; Martiarena, M. L. Abiotic degradation of glyphosate into aminomethyl phosphonic acid in the presence of metals. *J. Agric. Food Chem.* **2014**, *62*, 9651−9656.
(39) Prytz, Ø.; Flage-Larsen, E. The influence of exact exchange corrections in van der Waals layered narrow bandgap black phosphorus. *J. Phys.: Condens. Matter* **2009**, *22*, 015502−015510.
(40) Ta, H. T. T.; Tieu, A. K.; Zhu, H.; Yu, H.; Ta, T. D.; Wan, S.; Tran, N. V.; Le, H. M. Chemical origin of sodium phosphate interactions on iron and iron oxide surfaces by first principle calculations. *J. Phys. Chem. C* **2007**, *122*, 635−647.
(41) Tian, C.; Zhao, J.; Ou, X.; Wan, J.; Cai, Y.; Lin, Z.; Dang, Z.; Xing, B. Enhanced adsorption of p-arsanilic acid from water by amine-modified UiO-67 as examined using extended X-ray absorption fine structure, X-ray photoelectron spectroscopy, and density functional theory calculations. *Environ. Sci. Technol.* **2018**, *52*, 3466−3475.

NOTE ADDED AFTER ISSUE PUBLICATION

This paper was originally published on July 12, 2018, with a misspelling in the surname of the third author. The paper was reposted on July 18, 2018.

DOI: 10.1021/acsomega.8b00921
ACS Omega 2018, 3, 7832−7839